NANO LETTERS

pubs.acs.org/NanoLett

Letter

Artificial Graphene Spin Polarized Electrode for Magnetic Tunnel Junctions

Victor Zatko,* Regina Galceran, Marta Galbiati, Julian Peiro, Florian Godel, Lisa-Marie Kern, David Perconte, Fatima Ibrahim, Ali Hallal, Mairbek Chshiev, Benjamin Martinez, Carlos Frontera, Lluìs Balcells, Piran R. Kidambi, John Robertson, Stephan Hofmann, Sophie Collin, Frédéric Petroff, Marie-Blandine Martin, Bruno Dlubak,* and Pierre Seneor*

Cite This: *Nano Lett.* 2023, 23, 34–41

Read Online

ACCESS | Metrics & More | Article Recommendations

ABSTRACT: 2D materials offer the ability to expose their electronic structure to manipulations by a proximity effect. This could be harnessed to craft properties of 2D interfaces and van der Waals heterostructures in devices and quantum materials. We explore the possibility to create an artificial spin polarized electrode from graphene through proximity interaction with a ferromagnetic insulator to be used in a magnetic tunnel junction (MTJ). Ferromagnetic insulator/graphene artificial electrodes were fabricated and integrated in MTJs based on spin analyzers. Evidence of the emergence of spin polarization in proximitized graphene layers was observed through the occurrence of tunnel magnetoresistance. We deduced a spin dependent splitting of graphene's Dirac band structure (∼15 meV) induced by the proximity effect, potentially leading to full spin polarization and opening the way to gating. The extracted spin signals illustrate the potential of 2D quantum materials based on proximity effects to craft spintronics functionalities, from vertical MTJs memory cells to logic circuits.

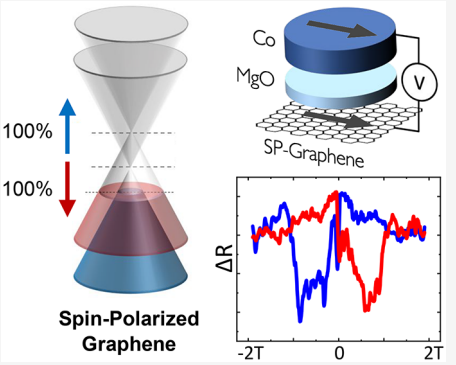

KEYWORDS: *proximity effects, 2D materials, graphene, spin polarization*

In recent years, spintronics has seen a rapid development of its application in data storage circuits, such as Magnetic Random Access Memories (MRAMs), targeting low energy cost and nonvolatility.[1,2] In this regard, spintronics already has emerged as a promising candidate for low power and more efficient electronics, as the spin degree of freedom naturally unifies memory functions with classical logic (in-memory logics), and even further with beyond CMOS technologies such as stochastic, neuromorphic, and quantum architectures.[3−7] This potential of spintronics is sustaining the quest for novel efficient and versatile material spin platforms. As such, introducing 2D materials in spintronics structures is foreseen to increase control over spin properties and extracted spin signals:[8,9] graphene, h-BN, and 2D semiconductors such as transition metal dichalcogenides have shown their ability for spin device tailoring (in terms of atomic thickness control, diffusion barrier in heterostructures, spin filtering, enhancement of magnetic anisotropy, spin orbit-toque effect...) while embedded in spin valves.[10−15]

In this direction, the use of 2D materials as a replacement for conventional spin sources could lead to improved control over device design. The basic building block of spintronics, the magnetic tunnel junction (MTJ), is made of two ferromagnetic spin sources separated by a thin insulating tunnel layer. Using bidimensional materials as a spin polarized electrode could provide sharp interfaces with a high tunability thanks to induced proximity effects and gating, leading to unprecedented control over carrier properties such as density and spin polarization. Pioneering studies started to use intrinsic 2D ferromagnets as spin polarized electrodes.[16] Interestingly, among 2D materials, graphene shows an impressive suitability for spintronics circuits with demonstrated efficient spin transport and spin filtering leading to high TMR ratios.[11,17,18] Furthermore, it exhibits low electrical resistivity and high stability to an ambient atmosphere. While graphene's band structure is not intrinsically spin dependent, magnetic proximity effects are expected to further provide an efficient control for band structure engineering as discussed in the case of lateral spin transport devices.[19−26] As a result of proximity effects, spin polarized graphene thus appears promising to

Received: August 5, 2022
Revised: November 24, 2022
Published: December 19, 2022

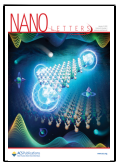

https://doi.org/10.1021/acs.nanolett.2c03113
Nano Lett. 2023, 23, 34−41

implement a 2D spin polarized conductive electrode in spin valve structures. These electrodes could then be used in vertical MTJ memory cells, and in lateral spin transport as well as logic circuits, paving the road toward an efficient universal material spin platform. Although theoretically predicted for graphene/magnetic insulator lateral devices, successful extraction of spins from proximitized graphene remains to be experimentally demonstrated in a vertical MTJ device configuration.[27]

In this Letter, we show that when graphene is at the vicinity of an insulating ferromagnetic layer, its intrinsic properties can be fundamentally changed into a spin polarized electrode through hybridization. Graphene can then be used as a spin source, here demonstrated in a reference MTJ. The study presented here is based on a graphene layer grown by chemical vapor deposition (CVD) transferred on top of the ferromagnetic insulator (FMI) LCoMO ($La_2Co_{1-x}Mn_{1+x}O_6$ ($x \sim 0.23$)). A graphene/LCoMO electrode is then integrated into spin valve structures to probe the spin dependent properties induced within the graphene layer by LCoMO (Figure 1). Magnetotransport measurements on such devices

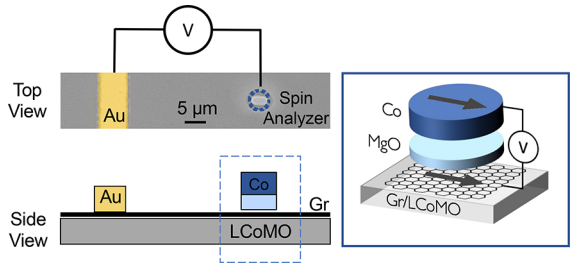

Figure 1. Optical image and schematic view of the devices. The image has been taken with a ×50 magnification objective. A microjunction is patterned on top of a LCoMO/graphene electrode. A top spin analyzer (Co/Oxide) is deposited to probe the spin polarization in graphene, leading to a magnetic tunnel junction. A gold contact is used to connect graphene.

show a magnetoresistive behavior that arises from the proximity effects between graphene and the FMI (Figure 2). Furthermore, a hysteretic spin transport signal is observed in several devices (Figure 3), demonstrating that graphene plays the role of an in-plane spin polarized electrode in this spin valve architecture, with spin polarization properties closely related to LCoMO's magnetic behavior. The origin of the obtained TMR spin signals is discussed, extracting the energy splitting in the graphene band structure due to exchange interaction with the FMI (Figure 4). We finally discuss the performance of these systems, highlighting conditions leading to almost full spin polarization, hence toward very high TMR spin signals beyond the current technological state of the art (Figure 5). These results illustrate the potential of the manipulation by proximity effects of spin dependent properties in graphene, toward an external control of the spin transport in graphene-based devices including both vertical MTJ and spin logic circuits.

Figure 1 presents the device structure: a 30 nm film of $La_2Co_{1-x}Mn_{1+x}O_6$ ($x \sim 0.23$) is sputtered on top of a LSAT (Lanthanum aluminate−Strontium Aluminum Tantalate) substrate as in ref 28. The strained state of the FMI results in an in-plane ferromagnetic insulator film. An O_2 plasma cleaning step is performed on the LCoMO surface to ensure an optimal oxygen content of the film before transferring the graphene layer on top.[29] The graphene layer is grown by CVD on Cu using a C_6H_6 precursor and then lifted and transferred onto a LCoMO substrate by standard transfer protocols using a poly(methyl methacrylate) (PMMA) carrier film.[30−32] In order to electrically isolate different devices within the same sample, individual graphene electrodes are defined by laser lithography and O_2 plasma etching. Another step of lithography is performed to design gold electrodes that are used to connect the graphene to a bias source. In order to define the top spin analyzer structure, a final lithography step is performed on top of the graphene/LCoMO electrode to define micrometer wide junctions: we grow a tunnel barrier (atomic layer deposition of 3 nm MgO or 1 nm sputtered Al_2O_3 depending on samples) and a top 15 nm sputtered Co ferromagnetic spin analyzer further capped with 80 nm Au.[33,34]

This fabrication process results in the definition of [LCoMO/Graphene]/oxide barrier/Co junctions, allowing us to probe proximity effects induced in graphene by LCoMO thanks to reference tunnel spin analyzers. A tunnel behavior is systematically measured on the junctions presented in this work by usual $I(V)$ and $dI/dV(V)$ measurements.[35,36,13] Graphene, on regular oxides, uncoupled to the environment,

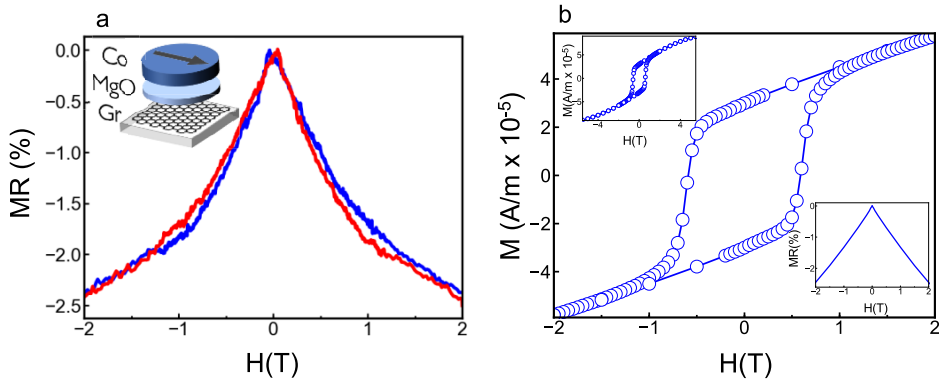

Figure 2. Magnetotransport measurements and simulations of the devices [LCoMO/Graphene]/MgO/Co. Inset: schematic of the device. (a) Experimental plot of the magnetoresistance (MR) as a function of in-plane external magnetic field at 2 K. The blue curve represents the measurement while sweeping from 2 T to −2 T, while the red curve is obtained when sweeping from −2 T to 2 T. We observe a clear negative MR and a hysteretic behavior below 1 T. (b) Raw SQUID data of the ferromagnetic insulator. Top inset shows SQUID data on a wider range (up to 5.5 T). Bottom inset shows simulations of the magnetoresistance of the devices.

https://doi.org/10.1021/acs.nanolett.2c03113
Nano Lett. 2023, 23, 34−41

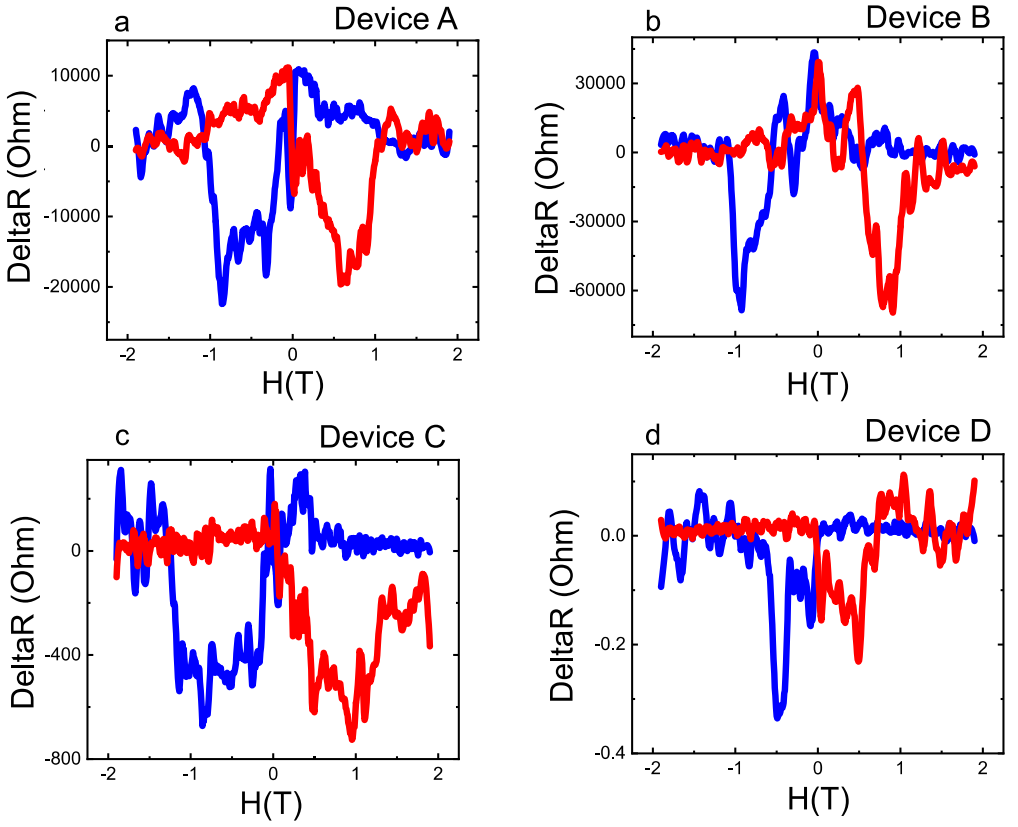

Figure 3. ΔR, the spin induced variation of the junction's resistance at 2 K, as a function of external in-plane magnetic field after subtraction of the general baseline. One can see a clear TMR signal: two distinct states of resistances are observed. This can be achieved only with 2 spin polarized electrodes, showing the spin polarization induced in the proximitized graphene. Devices A, B, and C are made with a MgO barrier while device D was made with an alumina barrier.

is not expected to provide a spin polarized current. Here, on the contrary, by the proximity with the ferromagnetic insulator substrate, we engineer a modification of graphene's band structure, lifting the degeneracy of the spin population densities. Experimentally, if the proximity effect is strong enough, it is expected to lead to the observation of a hysteretic behavior of the magnetoresistive signal corresponding to the classic response of a MTJ highlighting that the graphene layer has become spin polarized and acts as a spin source.

In Figure 2a we show typical in-plane magnetotransport measurements at 2 K for the devices with a MgO barrier. The resistance vs in-plane magnetic field curves of the junctions display a negative magnetoresistance (MR). This effect is not expected for an isolated graphene layer. Moreover, the current is applied between the graphene and the cobalt electrode. Importantly, it does not flow in or through the insulating LCoMO layer.[37] The insulating character of LCoMO was confirmed through DC transport measurement. Devices without the graphene electrode were found to be isolated with unmeasurable resistances (beyond the limit of our setup). Overall, the individual contributions of the isolated layers of the devices cannot explain the general trend of the magnetotransport, suggesting proximity effects between graphene and the FMI leading to the evolution of the graphene band structure. We note that our observed measurements can be ruled out as originating from spin-Hall effect (SHE) induced MR such as the spin-Hall magnetoresistance (SMR) effects arising at heavy metal/FMI interfaces.[38] Indeed, first graphene is acknowledged as a material with very low spin−orbit coupling, leading to vanishing SHE. Next, in a true 2D material, such as our single graphene layer, SHE would not create in-plane spins but would lead only to out-of-plane spins accumulating at the edges of graphene. Those out-of-plane spins would not be impacted by the reversal of our FMI's in-plane magnetization. Moreover, from the experimental point of view, the effects reported here are at least 1 order of magnitude higher than the highest resistance variation that could be expected from such SHE structures.

To further correlate the magnetotransport curve's general shape with proximity induced modification of graphene properties and model the magnetic field dependence, we show the raw in-plane SQUID measurement of a LCoMO film of the devices (Figure 2b). Above its coercive field, the magnetization of LCoMO smoothly aligns along the direction of the external magnetic field without being fully saturated even up to 5 T (the contribution of the LSAT substrate being diamagnetic, it cannot account for the increased magnetization with the externally applied magnetic field). As the spin polarization in graphene depends on the exchange interaction with the FMI which is proportional to its magnetization, the SQUID data associated with Jullière's model allow us to correlate the MR of our system with the application of an external in-plane magnetic field (more details are given below). Strikingly we are able to reproduce the overall evolution of the resistances with respect to an applied magnetic field as shown in the bottom inset of Figure 2b. The magnetotransport signal of the spin valves depends on the relative orientation of the magnetization of the two ferromagnets. As in the devices

https://doi.org/10.1021/acs.nanolett.2c03113
Nano Lett. 2023, 23, 34−41

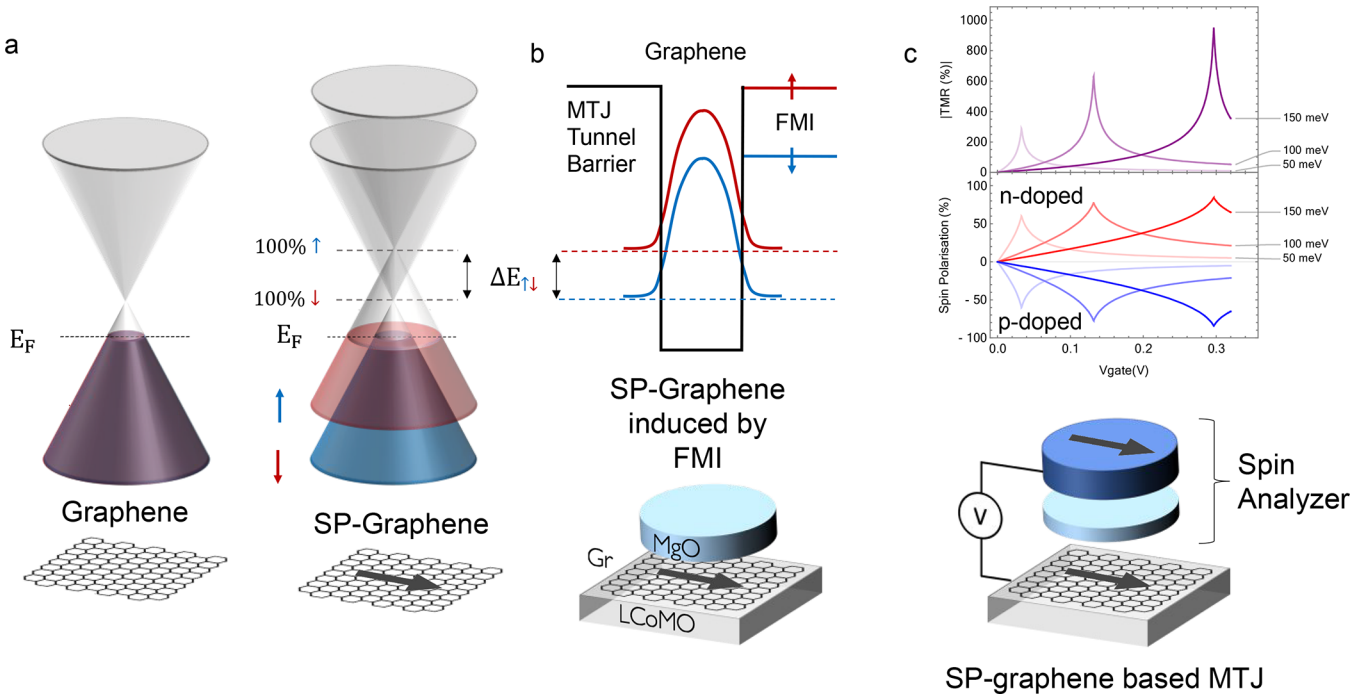

Figure 4. Model of the spin polarization induced in graphene through proximity effects with LCoMO. (a) Schematic of the splitting of the Dirac cones in graphene due to exchange with a ferromagnetic insulator (FMI). (b) Schematic representation of the splitting induced in graphene by proximity with an FMI and an oxide barrier in a MTJ. (c) Lower panel: Schematics of the resulting MTJ where the graphene plays the role of one of the spin polarized electrodes. Upper panel: TMR and spin polarization vs gate voltage induced by exchange interaction in a graphene in proximity with a ferromagnet for different values of exchange interaction. The peaks correspond to the extreme cases leading to an almost full spin polarization. If an additional small gap is opened in graphene at the Dirac point, the effect is even more dramatic.

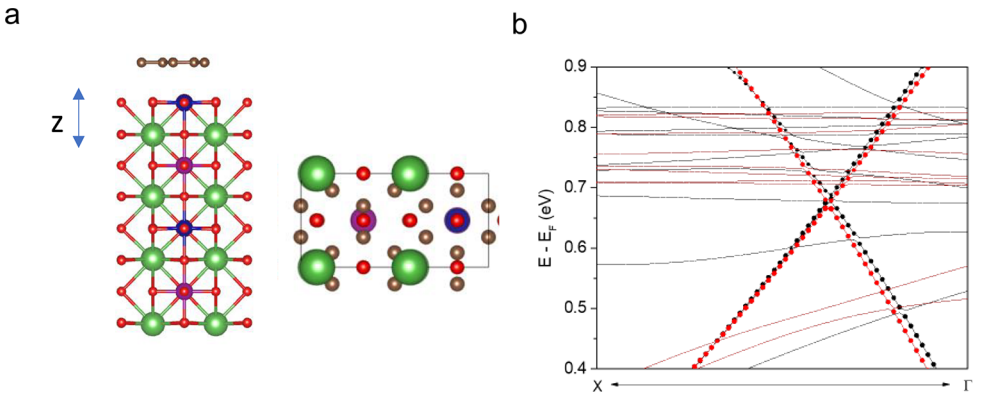

Figure 5. Electronic structure of the graphene layer at the Gr/LCOMO interface computed from first-principles. (a) Balls and sticks representation of the interface. Carbon, lanthane, cobalt, manganese, and oxygen atoms are depicted as brown, green, blue, violet, and red balls, respectively. (b) Spin splitted (black and red) electronic band structure of the graphene (solid circles) on top of LCoMO.

studied here, the top Co spin analyzer is fully aligned along the external in-plane magnetic field, the smooth alignment of the LCoMO along that same direction induces a smooth variation of the total resistance of the device (sensor-like behavior). In a nutshell, the observed MR is governed by the relative alignment of the top and bottom electrode magnetizations. The bottom artificial proximitized graphene electrode being induced by the LCoMO replicates its magnetization. As such, the observed inversed "parabolic-like" shape of the MR can be directly related to the LCoMO magnetization behavior observed in the presented additional SQUID magnetic characterizations (Figure 2b, top inset). The peculiar magnetic behavior of the insulting LCoMO layer has an effect on the spin transport of the full device through a proximity effect with graphene. The general behavior of the devices pinpoints a strong modification of graphene's intrinsic properties induced by the proximity with the FMI.

Besides the general magnetoresistive trend of the $R(H)$ curve (Figure 2a), a hysteretic behavior is also observed between 1 T and −1 T. We highlight these features by subtracting the general nonhysteretic magnetoresistance from the signal previously identified. The resulting hysteretic TMR signals for four different devices (devices A, B, C with MgO barrier and device D with alumina barrier) are presented in Figure 3. One can see that the extracted TMRs closely resemble the usual spin signals extracted from an MTJ with two metallic ferromagnets acting as spin polarized electrodes. However, here only one electrode is a conventional metallic

https://doi.org/10.1021/acs.nanolett.2c03113
Nano Lett. 2023, 23, 34−41

ferromagnet (Co), with the other electrode being graphene. As such, the otherwise nonmagnetic graphene appears to behave as a spin polarized electrode thanks to its interaction with the underlying FMI (LCoMO). The influence of the insulating LCoMO is further confirmed by the value of magnetic fields at which the hysteresis switches are observed in the TMR. These values match the LCoMO coercive field (Figure 2b).

The measured spin signal thus appears to arise from an extrinsic spin polarization induced within the graphene electrode by the proximity effect with the FMI. We can estimate this graphene spin polarization induced in graphene using Jullière's model and our Co-based spin analyzer stack. We have the tunneling magnetoresistance defined as $\mathrm{TMR} = \frac{2P_{\mathrm{analyzer}}P_{\mathrm{GrProx}}}{1 - P_{\mathrm{analyzer}}P_{\mathrm{GrProx}}}$ with P_{GrProx} and P_{analyzer} indicating the spin polarization of the graphene in proximity with LCoMO and the spin polarization of the Co-based spin analyzer, respectively. In an attempt to derive a lower bound for the induced characteristics of the graphene, we extract from previous works that $P_{\mathrm{analyzer}} \leq 32\%$ and from the measured TMR (~0.48%) we can deduce the spin polarization of the LCoMO-proximitized graphene $|P_{\mathrm{GrProx}}| \geq 0.8\%$.[39,40] We note that, in the case of sample D, the TMR signals were about 10 times smaller than for the other samples. This sample has been made with a sputtered 1 nm alumina tunnel barrier known to impact the graphene underneath whereas the others were made with a 3 nm ALD-deposited MgO tunnel barrier. The difference between both type of samples is consistent with the noninvasive higher quality of ALD grown barriers as noted in previous reports.[35,41] This observation is also consistent with the fact that the spin signal comes from the graphene embedded in the MTJ as we see the same general magnetotransport behavior with both tunnel barriers.

We now discuss the origin of the TMR signals observed in our devices and the related induced graphene spin polarization. The proximity with the ferromagnetic insulator LCoMO induces a spin dependent modification of the graphene band structure. This can be described in a first approximation by a spin dependent splitting ΔE of the Dirac band structure of graphene due to the proximity interaction with the FMI (as depicted in Figure 4a). While more complex in reality, a simple conceptual picture of this effect can be given by considering the graphene as an atom-thick quantum well (Figure 4b). When this atom-thin 2D quantum well is put into proximity with a FMI, its levels' degeneracy is lifted for the spin up and down directions. This is due to different barrier heights for the two spin directions in the FMI surrounding the quantum well (i.e., different evanescent waves in the FMI barrier). This leads to the exchange field of the FMI to be imprinted onto the 2D quantum well. A picture of our case, where we assume this effect to be homogeneous over the one atom-thick graphene height, is shown in Figure 4b. We can deduce the value of this splitting using the graphene spin polarization estimated from magnetotransport measurements. Indeed, the spin polarization can be defined as $P_{\mathrm{GrProx}}(E_{\mathrm{F}}) = \frac{D^{\uparrow}(E_{\mathrm{F}}) - D^{\downarrow}(E_{\mathrm{F}})}{D^{\uparrow}(E_{\mathrm{F}}) + D^{\downarrow}(E_{\mathrm{F}})}$, with $D^{\sigma}(E_{\mathrm{F}})$ being the graphene density of states for the spin direction $\sigma(\uparrow, \downarrow)$. Here we have $D^{\sigma}(E_{\mathrm{F}}) = \frac{E^{\sigma}}{\pi(\hbar v_{\mathrm{F}})^2}$ where $E^{\uparrow,\downarrow} = E_{\mathrm{F}} \pm \frac{\Delta E}{2}$ with $E_{\mathrm{F}} = \hbar v_{\mathrm{F}}\sqrt{\pi n}$ being the Fermi energy, n the carrier density, and V_{F} the Fermi velocity. From this, we deduce $P_{\mathrm{GrProx}}(E_{\mathrm{F}}) = \frac{E^{\uparrow} - E^{\downarrow}}{E^{\uparrow} + E^{\downarrow}}$ and find that the graphene spin polarization is directly linked to the exchange splitting by $P_{\mathrm{GrProx}}(E) = \frac{\Delta E}{2E_{\mathrm{F}}} = \frac{\Delta E}{2\hbar v_{\mathrm{F}}\sqrt{\pi n}}$. To give a first estimation of ΔE, we fabricated on the same chip a Hall bar device which allowed us to extract a carrier density of $n = -4 \times 10^{12}$ cm^{-2} for the graphene layer. Measurements of MTJ configurations based on reference spin analyzers Co/oxide described above highlight $P_{\mathrm{GrProx}}(E) \geq 0.8\%$. From this value, we can thus already infer an exchange splitting in graphene ΔE of at least 4 meV. However, following the SQUID data, we pinpoint that the observed induced exchange is related to the remanent magnetization of the FMI at its switching field of 0.8 T which is only 23% of its value at 5 T (see top inset of Figure 2b). Hence, at 5 T (almost saturated LCoMO), the expected induced exchange splitting is 15 meV. This qualitative approach is confirmed by first-principle calculations of the LCoMO/Gr interface where one finds the emergence of an induced exchange splitting—above 15 meV—in graphene associated with the presence of LCoMO. In this context, it clearly appears that a finely gated control of E_{F} might lead to a large P_{GrProx} for any given sizable splitting ΔE. This opportunity is illustrated in Figure 4c. In the extreme case where the Fermi level is aligned with the Dirac point of one spin direction through gating, the electronic density vanishes completely comparatively to the other spin direction; this leads to an artificial full spin polarization of the graphene. Here we note that while eventually the charge fluctuation Δn in graphene should be taken into account, this should not hamper the ability to achieve large spin polarization. Indeed, it was shown that charge fluctuations in the <10 meV range could be achieved even without requiring highly efficient h-BN passivation.[42] In this case, a splitting value of approximately 50 meV would already lead to more than 60% spin polarization, while an exchange splitting value of ~150 meV would lead to ~85% of spin polarization. It is worth noting that 60% of spin polarization corresponds to a TMR above 100%, while a spin polarization of 85% corresponds to TMR above 500%, the range usually observed with MgO tunnel barriers. Outstandingly, an even stronger effect could be achieved thanks to a proximity-effect induced gap in the graphene band structure at the Dirac point.[43] Indeed, such an induced gap would strongly suppress one of the spin directions, relaxing the impact of Δn, and leading to spin polarizations even closer to the ideal $P_{\mathrm{GrProx}} = 100\%$ case. It is important here to note that using a single layer, in addition to maximizing the impact of the proximity effect of the FMI on graphene, supports ruling out other thickness dependent effects.

These results illustrate the striking potential of the proximity effects to tailor the graphene toward modulated spintronics properties for MTJs and beyond for spin logics. The spin polarization could indeed be controlled through graphene gating leading to controllable spin polarizer/analyzer and spin torque properties. We think that this artificial FM proximitized graphene offers an interesting complement to the families of 2D ferromagnets (2D FMs) being now uncovered as spin sources.[44] Indeed, 2D FMs have been recently highlighted as offering very interesting potential compared to usual 3D systems, a key one being the gating of their FM properties.[45−49] As shown in Figure 4, our artificial system could also advantageously offer this gating potential, while, in contrast to 2D FMs, being easier to integrate. Indeed, 2D FM families still remain to be stabilized and developed (see for instance ref 50),

https://doi.org/10.1021/acs.nanolett.2c03113
Nano Lett. 2023, 23, 34−41

whereas graphene brings ambient stability and eased large scale fabrication. This is a clear asset for implementation that could furthermore benefit from the bright perspective to extract strong tunable spin polarizations from graphene. We note however that these assets are balanced by the fact that while numerous FMI are available, our approach requires engineering the right heterostructure while combining them with graphene. Still, the strong spin polarization dependence of such a system anticipated by our work suggests the implementation of a gate to take maximum benefit from it. Once the technological progress will allow such a geometry, a different path can be followed to reach the most pertinent system[51,7] such as direct backgating by adding a conductive layer below our graphene/FMI or by using both as a vertical and lateral spin source and exploiting the long spin lifetimes during transport in graphene to reach a second electrode. This would for example allow researchers to define a top gate structure on top of the graphene/FMI injection point and modulate the spin polarization as discussed. This would however be particularly demanding (spin transport is subtly dependent on device geometry and resistance matching, see ref 52), and we believe this will require a collective community-wide exploration.

In conclusion, we managed to convert graphene into a spin polarized electrode by proximity effects induced by an insulating ferromagnet layer and successfully implement it in functional MTJ structures. By analyzing the resulting sizable spin signals in several devices, we extract the energy splitting induced by FMI in the graphene band structure (∼15 meV) leading to the appearance of a spin polarization in graphene. This work expands the role that can be attributed to graphene in spintronics devices: it is demonstrated as a possible spin source in this proximitized configuration. Based on experimentally accessible materials and conditions with low charge fluctuations below 10 meV together with predictions of exchange splitting in the 100 meV range and gaps above 30 meV, spin polarizations above 75% are now foreseen in these systems.[43,53] This work opens broader perspectives toward fully 2D-based MTJs and van der Waals heterostructures that aim at exploiting the unique properties of 2D materials in spin transport. The spin polarization induced in graphene appears as an essential step toward all-spin logic circuits: bypassing the ferromagnet-channel impedance mismatch issue by selectively tailoring the same material either as a spin source or an efficient spin transport channel might finally lead to the well-looked after spin logic platform.[54,52]

AUTHOR INFORMATION

Corresponding Authors

Victor Zatko − *Unité Mixte de Physique, CNRS, Thales, Université Paris-Saclay, 91767 Palaiseau, France;* orcid.org/0000-0002-2475-8866; Email: victor.zatko@cnrs-thales.fr

Bruno Dlubak − *Unité Mixte de Physique, CNRS, Thales, Université Paris-Saclay, 91767 Palaiseau, France;* orcid.org/0000-0001-5696-8991; Email: bruno.dlubak@cnrs-thales.fr

Pierre Seneor − *Unité Mixte de Physique, CNRS, Thales, Université Paris-Saclay, 91767 Palaiseau, France*; Email: pierre.seneor@cnrs-thales.fr

Authors

Regina Galceran − *Unité Mixte de Physique, CNRS, Thales, Université Paris-Saclay, 91767 Palaiseau, France; CSIC and BIST, Campus UAB, Catalan Institute of Nanoscience and Nanotechnology (ICN2), Bellaterra 08193 Barcelona, Spain*

Marta Galbiati − *Unité Mixte de Physique, CNRS, Thales, Université Paris-Saclay, 91767 Palaiseau, France*

Julian Peiro − *Unité Mixte de Physique, CNRS, Thales, Université Paris-Saclay, 91767 Palaiseau, France*

Florian Godel − *Unité Mixte de Physique, CNRS, Thales, Université Paris-Saclay, 91767 Palaiseau, France;* orcid.org/0000-0003-1741-2741

Lisa-Marie Kern − *Unité Mixte de Physique, CNRS, Thales, Université Paris-Saclay, 91767 Palaiseau, France;* orcid.org/0000-0001-9781-9132

David Perconte − *Unité Mixte de Physique, CNRS, Thales, Université Paris-Saclay, 91767 Palaiseau, France*

Fatima Ibrahim − *Univ. Grenoble Alpes, CEA, CNRS, Spintec, 38000 Grenoble, France*

Ali Hallal − *Univ. Grenoble Alpes, CEA, CNRS, Spintec, 38000 Grenoble, France*

Mairbek Chshiev − *Univ. Grenoble Alpes, CEA, CNRS, Spintec, 38000 Grenoble, France; Institut Universitaire de France, 75231 Paris, France;* orcid.org/0000-0001-9232-7622

Benjamin Martinez − *Institut de Ciencia de Materials de Barcelona, ICMAB-CSIC, Campus UAB, 08193 Bellaterra, Spain*

Carlos Frontera − *Institut de Ciencia de Materials de Barcelona, ICMAB-CSIC, Campus UAB, 08193 Bellaterra, Spain;* orcid.org/0000-0002-0091-4756

Lluìs Balcells − *Institut de Ciencia de Materials de Barcelona, ICMAB-CSIC, Campus UAB, 08193 Bellaterra, Spain*

Piran R. Kidambi − *Department of Chemical and Biomolecular Engineering, Vanderbilt University, Nashville, Tennessee 37212, United States;* orcid.org/0000-0003-1546-5014

John Robertson − *Department of Engineering, University of Cambridge, Cambridge CB3 0FA, United Kingdom*

Stephan Hofmann − *Department of Engineering, University of Cambridge, Cambridge CB3 0FA, United Kingdom;* orcid.org/0000-0001-6375-1459

Sophie Collin − *Unité Mixte de Physique, CNRS, Thales, Université Paris-Saclay, 91767 Palaiseau, France*

Frédéric Petroff − *Unité Mixte de Physique, CNRS, Thales, Université Paris-Saclay, 91767 Palaiseau, France*

Marie-Blandine Martin − *Unité Mixte de Physique, CNRS, Thales, Université Paris-Saclay, 91767 Palaiseau, France*

Complete contact information is available at: https://pubs.acs.org/10.1021/acs.nanolett.2c03113

Notes

The authors declare no competing financial interest.

ACKNOWLEDGMENTS

This work has received funding from the European Union's H2020 Future and Emerging Technologies "Graphene Flagship" (Grant Core3 No. 881603), "SINFONIA" (No. 881603) projects and a Grant Agreement Marie Skłodowska Curie "ITN Spinograph" (No. 697904), as well as from EPSRC (EP/P005152/1, EP/K016636/1). This research is supported by a public grant overseen by the French National Research Agency

(ANR) as part of the "Investissements d'Avenir" program Labex NanoSaclay (ANR-10-LABX-0035), as well as grants STEM2D (ANR-19-CE24-0015), MIXES (ANR-19-CE09-0028), and by the Flag-ERA JTC 2019 project "SOGraph-MEM" (ANR-19-GRFI-0001-07). This work has also received fundings from the "Spanish ministry of Science and Innovation" through "Severo Ochoa" (CEX2019-000917-S) and "OXISOT" (PID2021-128410OB-I00).

REFERENCES

(1) Khvalkovskiy, A. V.; Apalkov, D.; Watts, S.; Chepulskii, R.; Beach, R. S.; Ong, A.; Tang, X.; Driskill-Smith, A.; Butler, W. H.; Visscher, P. B.; Lottis, D.; Chen, E.; Nikitin, V.; Krounbi, M. Basic Principles of STT-MRAM Cell Operation in Memory Arrays. *J. Phys. D. Appl. Phys.* **2013**, *46*, 074001.

(2) Dieny, B.; Prejbeanu, I. L.; Garello, K.; Gambardella, P.; Freitas, P.; Lehndorff, R.; Raberg, W.; Ebels, U.; Demokritov, S. O.; Akerman, J.; Deac, A.; Pirro, P.; Adelmann, C.; Anane, A.; Chumak, A. V.; Hirohata, A.; Mangin, S.; Valenzuela, S. O.; Onbasli, M. C.; d'Aquino, M.; Prenat, G.; Finocchio, G.; Lopez-Diaz, L.; Chantrell, R.; Chubykalo-Fesenko, O.; Bortolotti, P. Opportunities and Challenges for Spintronics in the Microelectronic Industry. *Nature Electronics* **2020**, *3*, 446.

(3) Behin-Aein, B.; Datta, D.; Salahuddin, S.; Datta, S. Proposal for an All-Spin Logic Device with Built-in Memory. *Nat. Nanotechnol.* **2010**, *5*, 266.

(4) Manipatruni, S.; Nikonov, D. E.; Lin, C. C.; Gosavi, T. A.; Liu, H.; Prasad, B.; Huang, Y. L.; Bonturim, E.; Ramesh, R.; Young, I. A. Scalable Energy-Efficient Magnetoelectric Spin−Orbit Logic. *Nature* **2019**, *565*, 35.

(5) Borders, W. A.; Pervaiz, A. Z.; Fukami, S.; Camsari, K. Y.; Ohno, H.; Datta, S. Integer Factorization Using Stochastic Magnetic Tunnel Junctions. *Nature* **2019**, *573*, 390.

(6) Grollier, J.; Querlioz, D.; Camsari, K. Y.; Everschor-Sitte, K.; Fukami, S.; Stiles, M. D. Neuromorphic Spintronics. *Nature Electronics* **2020**, *3*, 360.

(7) Khokhriakov, D.; Sayed, S.; Hoque, A. M.; Karpiak, B.; Zhao, B.; Datta, S.; Dash, S. P.Multifunctional Spin Logic Gates In Graphene Spin Circuits, *2021, 2108.12259, arXiv*,https://arxiv.org/abs/2108.12259 (accessed November 18th, 2022).

(8) Scharf, B.; Xu, G.; Matos-Abiague, A.; Žutić, I. Magnetic Proximity Effects in Transition-Metal Dichalcogenides: Converting Excitons. *Phys. Rev. Lett.* **2017**, *119*, 127403.

(9) Piquemal-Banci, M.; Galceran, R.; Martin, M. B.; Godel, F.; Anane, A.; Petroff, F.; Dlubak, B.; Seneor, P. 2D-MTJs: Introducing 2D Materials in Magnetic Tunnel Junctions. *J. Phys. D. Appl. Phys.* **2017**, *50*, 203002.

(10) Cobas, E. D.; Van 'T Erve, O. M. J.; Cheng, S. F.; Culbertson, J. C.; Jernigan, G. G.; Bussman, K.; Jonker, B. T. Room-Temperature Spin Filtering in Metallic Ferromagnet-Multilayer Graphene-Ferromagnet Junctions. *ACS Nano* **2016**, *10*, 10357.

(11) Piquemal-Banci, M.; Galceran, R.; Dubois, S. M. M.; Zatko, V.; Galbiati, M.; Godel, F.; Martin, M. B.; Weatherup, R. S.; Petroff, F.; Fert, A.; Charlier, J. C.; Robertson, J.; Hofmann, S.; Dlubak, B.; Seneor, P. Spin Filtering by Proximity Effects at Hybridized Interfaces in Spin-Valves with 2D Graphene Barriers. *Nat. Commun.* **2020**, *11*, 5670.

(12) Dankert, A.; Venkata Kamalakar, M.; Wajid, A.; Patel, R. S.; Dash, S. P. Tunnel Magnetoresistance with Atomically Thin Two-Dimensional Hexagonal Boron Nitride Barriers. *Nano Res. 2014 84* **2015**, *8*, 1357.

(13) Piquemal-Banci, M.; Galceran, R.; Godel, F.; Caneva, S.; Martin, M. B.; Weatherup, R. S.; Kidambi, P. R.; Bouzehouane, K.; Xavier, S.; Anane, A.; Petroff, F.; Fert, A.; Dubois, S. M. M.; Charlier, J. C.; Robertson, J.; Hofmann, S.; Dlubak, B.; Seneor, P. Insulator-to-Metallic Spin-Filtering in 2D-Magnetic Tunnel Junctions Based on Hexagonal Boron Nitride. *ACS Nano* **2018**, *12*, 4712.

(14) Dankert, A.; Pashaei, P.; Kamalakar, M. V.; Gaur, A. P. S.; Sahoo, S.; Rungger, I.; Narayan, A.; Dolui, K.; Hoque, M. A.; Patel, R. S.; de Jong, M. P.; Katiyar, R. S.; Sanvito, S.; Dash, S. P. Spin-Polarized Tunneling through Chemical Vapor Deposited Multilayer Molybdenum Disulfide. *ACS Nano* **2017**, *11*, 6389.

(15) Zatko, V.; Galbiati, M.; Dubois, S. M.-M.; Och, M.; Palczynski, P.; Mattevi, C.; Brus, P.; Bezencenet, O.; Martin, M.-B.; Servet, B.; Charlier, J.-C.; Godel, F.; Vecchiola, A.; Bouzehouane, K.; Collin, S.; Petroff, F.; Dlubak, B.; Seneor, P. Band-Structure Spin-Filtering in Vertical Spin Valves Based on Chemical Vapor Deposited WS_2. *ACS Nano* **2019**, *13*, 14468.

(16) Wang, Z.; Gutiérrez-Lezama, I.; Ubrig, N.; Kroner, M.; Gibertini, M.; Taniguchi, T.; Watanabe, K.; Imamoğlu, A.; Giannini, E.; Morpurgo, A. F. Very Large Tunneling Magnetoresistance in Layered Magnetic Semiconductor CrI3. *Nat. Commun.* **2018**, *9*, 2516.

(17) Karpan, V. M.; Giovannetti, G.; Khomyakov, P. A.; Talanana, M.; Starikov, A. A.; Zwierzycki, M.; van den Brink, J.; Brocks, G.; Kelly, P. J. Graphite and Graphene as Perfect Spin Filters. *Phys. Rev. Lett.* **2007**, *99*, 176602.

(18) Dlubak, B.; Martin, M.-B.; Deranlot, C.; Servet, B.; Xavier, S.; Mattana, R.; Sprinkle, M.; Berger, C.; De Heer, W. A.; Petroff, F.; Anane, A.; Seneor, P.; Fert, A. Highly Efficient Spin Transport in Epitaxial Graphene on SiC. *Nat. Phys.* **2012**, *8*, 557.

(19) Leutenantsmeyer, J. C.; Kaverzin, A. A; Wojtaszek, M.; van Wees, B. J Proximity Induced Room Temperature Ferromagnetism in Graphene Probed with Spin Currents. *2D Mater.* **2017**, *4*, 014001.

(20) Wang, Z.; Tang, C.; Sachs, R.; Barlas, Y.; Shi, J. Proximity-Induced Ferromagnetism in Graphene Revealed by the Anomalous Hall Effect. *Phys. Rev. Lett.* **2015**, *114*, 016603.

(21) Wu, Y. F.; Song, H. D.; Zhang, L.; Yang, X.; Ren, Z.; Liu, D.; Wu, H. C.; Wu, J.; Li, J. G.; Jia, Z.; Yan, B.; Wu, X.; Duan, C. G.; Han, G.; Liao, Z. M.; Yu, D. Magnetic Proximity Effect in Graphene Coupled to a BiFe O3 Nanoplate. *Phys. Rev. B* **2017**, *95*, 195426.

(22) Wei, P.; Lee, S.; Lemaitre, F.; Pinel, L.; Cutaia, D.; Cha, W.; Katmis, F.; Zhu, Y.; Heiman, D.; Hone, J.; Moodera, J. S.; Chen, C. T. Strong Interfacial Exchange Field in the Graphene/EuS Heterostructure. *Nat. Mater.* **2016**, *15*, 711.

(23) Tang, C.; Zhang, Z.; Lai, S.; Tan, Q.; Gao, W. Magnetic Proximity Effect in Graphene/$CrBr_3$ van Der Waals Heterostructures. *Adv. Mater.* **2020**, *32*, 1908498.

(24) Ghiasi, T. S.; Kaverzin, A. A.; Dismukes, A. H.; de Wal, D. K.; Roy, X.; van Wees, B. J. Electrical and Thermal Generation of Spin Currents by Magnetic Bilayer Graphene. *Nat. Nanotechnol. 2021 167* **2021**, *16*, 788.

(25) Karpiak, B.; Cummings, A. W.; Zollner, K.; Vila, M.; Khokhriakov, D.; Hoque, A. M.; Dankert, A.; Svedlindh, P.; Fabian, J.; Roche, S.; Dash, S. P. Magnetic Proximity in a van Der Waals Heterostructure of Magnetic Insulator and Graphene. *2D Mater.* **2020**, *7*, 015026.

(26) Kaverzin, A. A; Ghiasi, T. S; Dismukes, A. H; Roy, X.; van Wees, B. J Spin Injection by Spin−Charge Coupling in Proximity Induced Magnetic Graphene. *2D Mater.* **2022**, *9*, 045003.

(27) Solis, D. A.; Hallal, A.; Waintal, X.; Chshiev, M. Proximity Magnetoresistance in Graphene Induced by Magnetic Insulators. *Phys. Rev. B* **2019**, *100*, 104402.

(28) Galceran, R.; López-Mir, L.; Bozzo, B.; Cisneros-Fernández, J.; Santiso, J.; Balcells, L.; Frontera, C.; Martínez, B. Strain-Induced Perpendicular Magnetic Anisotropy in L A2CoMn O6-É Thin Films and Its Dependence on Film Thickness. *Phys. Rev. B* **2016**, *93*, 144417.

(29) Galceran, R.; Frontera, C.; Balcells, L.; Cisneros-Fernández, J.; López-Mir, L.; Roqueta, J.; Santiso, J.; Bagués, N.; Bozzo, B.; Pomar, A.; Sandiumenge, F.; Martínez, B. Engineering the Microstructure and Magnetism of La2CoMnO6-δ Thin Films by Tailoring Oxygen Stoichiometry. *Appl. Phys. Lett.* **2014**, *105*, 242401.

(30) Kidambi, P. R.; Ducati, C.; Dlubak, B.; Gardiner, D.; Weatherup, R. S.; Martin, M. B.; Seneor, P.; Coles, H.; Hofmann, S. The Parameter Space of Graphene Chemical Vapor Deposition on Polycrystalline Cu. *J. Phys. Chem. C* **2012**, *116*, 22492.

https://doi.org/10.1021/acs.nanolett.2c03113
Nano Lett. 2023, 23, 34−41

(31) Dlubak, B.; Kidambi, P. R.; Weatherup, R. S.; Hofmann, S.; Robertson, J. Substrate-Assisted Nucleation of Ultra-Thin Dielectric Layers on Graphene by Atomic Layer Deposition. *Appl. Phys. Lett.* **2012**, *100*, 173113.
(32) Mzali, S.; Montanaro, A.; Xavier, S.; Servet, B.; Mazellier, J. P.; Bezencenet, O.; Legagneux, P.; Piquemal-Banci, M.; Galceran, R.; Dlubak, B.; Seneor, P.; Martin, M. B.; Hofmann, S.; Robertson, J.; Cojocaru, C. S.; Centeno, A.; Zurutuza, A. Stabilizing a Graphene Platform toward Discrete Components. *Appl. Phys. Lett.* **2016**, *109*, 253110.
(33) Kern, L. M.; Galceran, R.; Zatko, V.; Galbiati, M.; Godel, F.; Perconte, D.; Bouamrane, F.; Gaufrès, E.; Loiseau, A.; Brus, P.; Bezencenet, O.; Martin, M. B.; Servet, B.; Petroff, F.; Dlubak, B.; Seneor, P. Atomic Layer Deposition of a MgO Barrier for a Passivated Black Phosphorus Spintronics Platform. *Appl. Phys. Lett.* **2019**, *114*, 053107.
(34) Dlubak, B.; Martin, M. B.; Deranlot, C.; Bouzehouane, K.; Fusil, S.; Mattana, R.; Petroff, F.; Anane, A.; Seneor, P.; Fert, A. Homogeneous Pinhole Free 1 Nm Al2O3 Tunnel Barriers on Graphene. *Appl. Phys. Lett.* **2012**, *101*, 203104.
(35) Dlubak, B.; Martin, M.-B.; Weatherup, R. S.; Yang, H.; Deranlot, C.; Blume, R.; Schloegl, R.; Fert, A.; Anane, A.; Hofmann, S.; Seneor, P.; Robertson, J. Graphene-Passivated Nickel as an Oxidation-Resistant Electrode for Spintronics. *ACS Nano* **2012**, *6*, 10930.
(36) Martin, M. B.; Dlubak, B.; Weatherup, R. S.; Piquemal-Banci, M.; Yang, H.; Blume, R.; Schloegl, R.; Collin, S.; Petroff, F.; Hofmann, S.; Robertson, J.; Anane, A.; Fert, A.; Seneor, P. Protecting Nickel with Graphene Spin-Filtering Membranes: A Single Layer Is Enough. *Appl. Phys. Lett.* **2015**, *107*, 012408.
(37) Lopez-Mir, L.; Frontera, C.; Aramberri, H.; Bouzehouane, K.; Cisneros-Fernandez, J.; Bozzo, B.; Balcells, L.; Martinez, B. Anisotropic Sensor and Memory Device with a Ferromagnetic Tunnel Barrier as the Only Magnetic Element OPEN. *Sci. Rep.* **2018**, *8*, 861.
(38) Nakayama, H.; Althammer, M.; Chen, Y. T.; Uchida, K.; Kajiwara, Y.; Kikuchi, D.; Ohtani, T.; Geprägs, S.; Opel, M.; Takahashi, S.; Gross, R.; Bauer, G. E. W.; Goennenwein, S. T. B.; Saitoh, E. Spin Hall Magnetoresistance Induced by a Nonequilibrium Proximity Effect. *Phys. Rev. Lett.* **2013**, *110*, 206601.
(39) Bernand-Mantel, A.; Seneor, P.; Lidgi, N.; Muñoz, M.; Cros, V.; Fusil, S.; Bouzehouane, K.; Deranlot, C.; Vaures, A.; Petroff, F.; Fert, A. Evidence for Spin Injection in a Single Metallic Nanoparticle: A Step towards Nanospintronics. *Appl. Phys. Lett.* **2006**, *89*, 062502.
(40) Barraud, C.; Deranlot, C.; Seneor, P.; Mattana, R.; Dlubak, B.; Fusil, S.; Bouzehouane, K.; Deneuve, D.; Petroff, F.; Fert, A. Magnetoresistance in Magnetic Tunnel Junctions Grown on Flexible Organic Substrates. *Appl. Phys. Lett.* **2010**, *96*, 072502.
(41) Martin, M. B.; Dlubak, B.; Weatherup, R. S.; Yang, H.; Deranlot, C.; Bouzehouane, K.; Petroff, F.; Anane, A.; Hofmann, S.; Robertson, J.; Fert, A.; Seneor, P. Sub-Nanometer Atomic Layer Deposition for Spintronics in Magnetic Tunnel Junctions Based on Graphene Spin-Filtering Membranes. *ACS Nano* **2014**, *8*, 7890.
(42) He, H.; Kim, K. H.; Danilov, A.; Montemurro, D.; Yu, L.; Park, Y. W.; Lombardi, F.; Bauch, T.; Moth-Poulsen, K.; Iakimov, T.; Yakimova, R.; Malmberg, P.; Müller, C.; Kubatkin, S.; Lara-Avila, S. Uniform Doping of Graphene Close to the Dirac Point by Polymer-Assisted Assembly of Molecular Dopants. *Nat. Commun.* **2018**, *9*, 3956.
(43) Yang, H. X.; Hallal, A.; Terrade, D.; Waintal, X.; Roche, S.; Chshiev, M. Proximity Effects Induced in Graphene by Magnetic Insulators: First-Principles Calculations on Spin Filtering and Exchange-Splitting Gaps. *Phys. Rev. Lett.* **2013**, *110*, 046603.
(44) Zhao, B.; Ngaloy, R.; Hoque, A. M.; Karpiak, B.; Khokhriakov, D.; Dash, S. P.Van Der Waals Magnet Based Spin-Valve Devices at Room Temperature, *2021, 2107.00310, arXiv*, https://arxiv.org/abs/2107.00310 (accessed November 18th, 2022).
(45) Deng, Y.; Yu, Y.; Song, Y.; Zhang, J.; Wang, N. Z.; Sun, Z.; Yi, Y.; Wu, Y. Z.; Wu, S.; Zhu, J.; Wang, J.; Chen, X. H.; Zhang, Y. Gate-Tunable Room-Temperature Ferromagnetism in Two-Dimensional Fe3GeTe2. *Nat. 2018 5637729* **2018**, *563*, 94.
(46) Wang, K.; De Greve, K.; Jauregui, L. A.; Sushko, A.; High, A.; Zhou, Y.; Scuri, G.; Taniguchi, T.; Watanabe, K.; Lukin, M. D.; Park, H.; Kim, P. Electrical Control of Charged Carriers and Excitons in Atomically Thin Materials. *Nat. Nanotechnol. 2018 132* **2018**, *13*, 128.
(47) Gibertini, M.; Koperski, M.; Morpurgo, A. F.; Novoselov, K. S. Magnetic 2D Materials and Heterostructures. *Nat. Nanotechnol. 2019 145* **2019**, *14*, 408.
(48) Och, M.; Martin, M. B.; Dlubak, B.; Seneor, P.; Mattevi, C. Synthesis of Emerging 2D Layered Magnetic Materials. *Nanoscale* **2021**, *13*, 2157.
(49) Yang, H.; Valenzuela, S. O.; Chshiev, M.; Couet, S.; Dieny, B.; Dlubak, B.; Fert, A.; Garello, K.; Jamet, M.; Jeong, D. E.; Lee, K.; Lee, T.; Martin, M. B.; Kar, G. S.; Sénéor, P.; Shin, H. J.; Roche, S. Two-Dimensional Materials Prospects for Non-Volatile Spintronic Memories. *Nat. 2022 6067915* **2022**, *606*, 663.
(50) Galbiati, M.; Zatko, V.; Godel, F.; Hirschauer, P.; Vecchiola, A.; Bouzehouane, K.; Collin, S.; Servet, B.; Cantarero, A.; Petroff, F.; Martin, M. B.; Dlubak, B.; Seneor, P. Very Long Term Stabilization of a 2D Magnet down to the Monolayer for Device Integration. *ACS Appl. Electron. Mater.* **2020**, *2*, 3508.
(51) Wen, H.; Dery, H.; Amamou, W.; Zhu, T.; Lin, Z.; Shi, J.; Žutić, I.; Krivorotov, I.; Sham, L. J.; Kawakami, R. K. Experimental Demonstration of Xor Operation in Graphene Magnetologic Gates at Room Temperature. *Phys. Rev. Appl.* **2016**, *5*, 044003.
(52) Seneor, P.; Dlubak, B.; Martin, M. B.; Anane, A.; Jaffres, H.; Fert, A. Spintronics with Graphene. *MRS Bull.* **2012**, *37*, 1245.
(53) Holmes, A. M.; Pakniyat, S.; Gangaraj, S. A. H.; Monticone, F.; Weinert, M.; Hanson, G. W. Exchange Splitting and Exchange-Induced Nonreciprocal Photonic Behavior of Graphene in CrI3-Graphene van Der Waals Heterostructures. *Phys. Rev. B* **2020**, *102*, 075435.
(54) Fert, A.; Jaffrès, H. Conditions for Efficient Spin Injection from a Ferromagnetic Metal into a Semiconductor. *Phys. Rev. B - Condens. Matter Mater. Phys.* **2001**, *64*, 184420.

https://doi.org/10.1021/acs.nanolett.2c03113
Nano Lett. 2023, 23, 34−41